Available online at www.sciencedirect.com
SCIENCE DIRECT®
Ocean Modelling 9 (2005) 305–323
Ocean Modelling
www.elsevier.com/locate/ocemod

Numerical modeling of wind waves generated by tropical cyclones using moving grids ☆

Hendrik L. Tolman *, Jose-Henrique G.M. Alves

SAIC-GSO at NOAA/NCEP/EMC Marine Modeling and Analysis Branch, 5200 Auth Road Room 209, Camp Springs, MD 20746, USA

Received 16 March 2004; received in revised form 11 August 2004; accepted 13 September 2004
Available online 2 November 2004

Abstract

A version of the WAVEWATCH III wave model featuring a continuously moving spatial grid is presented. The new model option/version is intended for research into wind waves generated by tropical cyclones in deep water away from the coast. The main advantage of such an approach is that the cyclones can be modeled with spatial grids that cover much smaller areas than conventional fixed grids, making model runs with high spatial resolution more economically feasible. The model modifications necessary are fairly trivial. Most complications occur due to the Garden Sprinkler effect (GSE) and methods used to mitigate it. The basic testing of the model is performed using idealized wind fields consisting of a Rankine vortex. The model is also applied to hurricane Lili in the Gulf of Mexico in October 2002. The latter application shows that the moving grid approach provides a natural way to deal with hurricane wind fields that have a high-resolution in space, but a low resolution in time. Although the new model version is originally intended for tropical cyclones, it is suitable for high-resolution modeling of waves due to any moving weather pattern.

Keywords: Wind waves; Tropical cyclones; Numerical modeling; Moving grids; Hurricane Lili

☆ MMAB contribution No. 240.

* Corresponding author. Tel.: +1 301 763 8000x7253; fax: +1 301 763 8545.
E-mail addresses: hendrik.tolman@noaa.gov (H.L. Tolman), henrique.alves@noaa.gov (J-H.G.M. Alves).

1463-5003/$ - see front matter © 2004 Published by Elsevier Ltd.
doi:10.1016/j.ocemod.2004.09.003

1. Introduction

Modeling and prediction of tropical cyclones has been in the center of attention for many years because of their potential to cause severe damage to life and property. Apart from high wind speeds and increased mean water levels at landfall, wave heights associated with tropical cyclones pose a major hazard. Accurate modeling of wind waves generated by hurricanes is, therefore, of great importance for emergency management purposes (e.g., Phadke et al., 2003).

One of the major problems for numerical modeling of waves generated by tropical cyclones is the small scale structure of such cyclones, which requires high model resolutions in space and time. In atmospheric modeling of tropical cyclones this has lead to well established nesting techniques, where high-resolution grids move with the tropical system within larger domains with lower resolution (for instance Kurihara et al., 1979; Kurihara and Bender, 1980; Bender et al., 1993; Kurihara et al., 1995). High and low resolution grids fully exchange information, and the high-resolution grids are regularly relocated, giving the impression of moving nests. However, the nests themselves are simply relocated to match the position of the cyclone, without considering actual motion of the grids. Whereas successful applications with other adaptive grid schemes (e.g., Gopalakrishnan et al., 2002) have been made, this 'jumping grid' approach still appears the method of choice for locally increasing model resolution around tropical systems in atmospheric modeling.

Recent research into the prediction of tropical cyclones also indicates the need for coupling atmospheric models with ocean models (e.g., Bender and Ginis, 2000) and with wave models (e.g., Bao et al., 2000). Coupling with the ocean is required to dynamically adjust sea surface temperatures (and hence ocean-atmosphere fluxes). Coupling with wave models is required to dynamically adjust the surface roughness, and possibly mass transport through the boundary layer (e.g., Chalikov and Belevich, 1993; Bao et al., 2000).

Somewhat surprisingly, the amount of attention paid to wave modeling for tropical cyclones is much less than for the atmosphere or storm surges. With the exemption of earlier work by Young (1988, 1999, 2003), most publications on wave modeling for tropical cyclones have been fairly recent (e.g., Chao and Tolman, 2000, 2001; Chao et al., 2003; Phadke et al., 2003; Moon et al., 2003). These recent numerical studies suffer from the fact the wave models do not share the 'jumping nest' capability of the atmospheric models. Hence, these studies utilize large high-resolution grids, whereas the high-resolution is only needed near the tropical cyclone. Due to this uneconomical approach, the attainable resolution is limited.

Ideally, it is desirable to use the relocatable nest technology from the atmospheric models in wave models. This would allow for the use of full resolution wind fields in wave models, and avoid the need for interpolating wave data back to the grid of the atmospheric model. This however, requires a major technological effort. Although such efforts are considered for implementation in some wave models, this technology is not expected to be available in the near future.

As an alternative to model wave conditions near a tropical system at sufficiently high spatial resolution, a continuously moving grid version of the WAVEWATCH III model (Tolman, 1991; Tolman et al., 2002; Tolman, 2002b) has been developed. This model is mostly intended for tropical cyclone research in idealized conditions, as outlined below. To simplify the moving grid approach, the resulting model is set up for deep water without coastlines only. With such an approach, a relatively small high resolution grid can be moved with the tropical cyclone, thus

making high resolution wave model calculations feasible. Because the resulting models are expected to cover relatively small areas, the modifications of WAVEWATCH III are furthermore only made for the Cartesian grid version of the model.

This model will first be used to revisit Young's parametric hurricane wave model (Young, 1988), as will be reported elsewhere. It is furthermore intended to investigate the sensitivity of hurricane wave prediction to grid resolutions, and possible refinements of numerical approaches and physical parameterizations (including coupling with ocean and atmosphere models), while a generally applicable jumping nest approach with full interaction of nests is being developed for WAVEWATCH III.

The moving grid approach provides a natural way to use high-resolution wind field analyses for hurricanes in wave modeling. Such modeling efforts are usually hampered by the fact that these wind fields have excellent spatial resolution, but poor temporal resolution. This will be illustrated here with some practical examples for hurricane Lili in the Gulf of Mexico in October 2002.

The outline of this paper is as follows. In Section 2, the general concept of the moving grid model is discussed. Section 3 focuses on aspects of the numerical implementation, with special attention on alleviating the Garden Sprinkler effect in Section 4. In Section 5, results of several idealized test cases are presented, and in Section 6 the new model is applied to hurricane Lili. Section 7 presents a discussion and conclusions.

2. General concept

Ocean wave models like WAVEWATCH III are generally based on a spectral action of energy balance equation

$$\frac{\partial F(f,\theta)}{\partial t} + \nabla_x \cdot \vec{c}_x F(f,\theta) + \nabla_{f,\theta} \cdot \vec{c}_{f,\theta} F(f,\theta) = S(f,\theta), \tag{1}$$

where f and θ are the spectral frequency and direction, respectively, F is the spectrum, $\vec{c}_x$ and $\vec{c}_{f,\theta}$ are the characteristics velocities in the physical and spectral space, respectively, and ∇_x and $\nabla_{f,\theta}$ are the corresponding gradient differential operators. The second term on the left describes effects of spatial propagation, the third term describes shifts in frequency and direction within the spectrum. The term S on the right side represents the net contribution of sources and sinks (wind, non-linearities, wave breaking and shallow water processes). A more detailed description of the balance equation can be found in, for instance, Komen et al. (1994), Young (1999), or Tolman (2002b).

Normally Eq. (1) is solved for a (fixed) non-moving spatial grid. Moving the computational grid with the velocity $\vec{v}$ simply advects the model solution with the velocity $-\vec{v}$ relative to the moving grid. The balance equation (1) relative to the moving grid thus becomes

$$\frac{\partial F(f,\theta)}{\partial t} + \nabla_x \cdot (\vec{c}_x - \vec{v}) F(f,\theta) + \nabla_{f,\theta} \cdot \vec{c}_{f,\theta} F(f,\theta) = S(f,\theta). \tag{2}$$

Note that the frame of reference for individual waves remains the same, and that the movement of the spatial grid only represent a movement of the part of the ocean which is observed by the model. Hence, source term formulations remain unchanged, and $\vec{v}$ is homogeneous, but can vary

in time. From a mathematical perspective, there are no constraints for $\vec{v}$. For practical hurricane modeling, $\vec{v}$ ideally represents the movement of the hurricane. It can be part of a parametric description of a hurricane, or can be deduced from observations or (hurricane wind) models.

Although the modification in Eq. (2) is simple in mathematical terms, several numerical complications are introduced. For instance, the bathymetry changes in time relative to the moving grid, as do the characteristic velocities in spectral space. Most wave models are not set up to account for this. Furthermore, islands and coastlines now become non-stationary rather than stationary internal boundaries. Although it is not expected that these complications will pose insurmountable problems, they require major changes to the structure of a wave model. In its general form, Eq. (2) thus does not provide a simple procedure to examine waves generated by tropical cyclones.

The numerical complications, as mentioned above, are related to the movement of the bathymetry and coastlines relative to the moving grid. None of these complications occur in deep water away from the coastline. A research tool for deep water conditions away from the coast is therefore much more easily developed. For such conditions, the third term on the left side of Eq. (2) only retains terms describing the change of direction when following great circles on a sphere. These terms also disappear when the solution is calculated on a flat (Cartesian) grid. In view of these possible simplifications, the present study focuses on the elementary problem of deep water waves on Cartesian grids without land masses, and the corresponding balance equation becomes

$$\frac{\partial F(f,\theta)}{\partial t} + (\vec{c}_x - \vec{v}) \cdot \nabla_x F(f,\theta) = S(f,\theta). \tag{3}$$

3. Numerical implementation

The moving grid approach has been introduced in the WAVEWATCH III wave model (Tolman, 1991; Tolman et al., 2002; Tolman, 2002b). This model solves the wave action balance equation similar to Eq. (1), for a spectrum defined in terms of the wave number k and direction θ. The model output spectra, however, are converted into variance (energy) density spectra as a function of frequency f and direction θ as in the latter equation. For the deep water conditions (without currents) considered here, the two sets of equations are equivalent.

WAVEWATCH III solves spatial propagation with either a simple first order scheme or with the third order ULTIMATE QUICKEST (UQ) scheme (Leonard, 1979, 1991). The moving grid approach is implemented by replacing the advection velocity in physical space ($\vec{c}_x$) with $\vec{c}_x - \vec{v}$ as in Eqs. (2) or (3). Such a modification is trivial in the wave model code, once the user defined advection velocity $\vec{v}(t)$ is made available to the proper propagation routines.

Three additional considerations have been made while including the moving grid option in WAVEWATCH III.

(1) The wave model requires a user-defined maximum propagation time step for the fastest moving spectral component. For all other spectral components the maximum allowed time step is adjusted by the ratio of the characteristic velocity for which the user-defined time step is given, to the actual characteristic velocity of the spectral component considered, (see Eq. (3.4) of

Tolman, 2002b). To avoid the need to adjust time steps as a function of $\vec{v}$, the internally calculated time step is automatically adjusted by considering the appropriate characteristic velocity $\vec{c}_x - \vec{v}$, assuming that the user-defined time step is valid for $\vec{v} \equiv 0$.

(2) All tests considered in the moving grid version of WAVEWATCH III are by definition limited area models. For such models, boundary conditions are required at the outer limits of the grid. No changes are made to the model code to account for moving boundaries. This implies that the user can either use the standard absorbing boundaries, or can define (constant) boundary conditions as described in the wave model manual. The first option will generally be sufficient, because the moving grid model will generally be used to assess the'near field' solution of the tropical cyclone. However, it is also possible to define background wave fields through the standard WAVEWATCH III methods to define boundary conditions.

(3) Numerical wave models with accurate numerical propagation schemes are subject to the Garden Sprinkler effect (GSE). This implies that the coarse spectral discretization results in a disintegration of continuous swell fields into discrete swell fields (see Booij and Holthuijsen, 1987; Tolman, 2002a). Alleviating the GSE in the moving grid version of the model will be discussed in detail in the following section.

4. The Garden Sprinkler effect

To alleviate the GSE, Booij and Holthuijsen (1987) have suggested a modified version of Eq. (3) that explicitly accounts for the sub-grid dispersion of the swell field. This is achieved by adding a diffusion tensor to the spatial propagation term in the balance equation

$$\frac{\partial F}{\partial t} + \frac{\partial}{\partial x}\left[c_x F - D_{xx}\frac{\partial F}{\partial x}\right] + \frac{\partial}{\partial y}\left[c_y F - D_{yy}\frac{\partial F}{\partial y}\right] - 2D_{xy}\frac{\partial^2 F}{\partial x \partial y} = S, \tag{4}$$

$$D_{xx} = D_{ss}\cos^2\theta + D_{nn}\sin^2\theta, \tag{5}$$

$$D_{yy} = D_{ss}\sin^2\theta + D_{nn}\cos^2\theta, \tag{6}$$

$$D_{xy} = (D_{ss} - D_{nn})\cos\theta\sin\theta, \tag{7}$$

$$D_{ss} = (\Delta c_g)^2 T_s/12, \tag{8}$$

$$D_{nn} = (c_g \Delta\theta)^2 T_s/12, \tag{9}$$

where D_{ss} is the diffusion coefficient in the propagation direction of the discrete wave component, D_{nn} is the diffusion coefficient along the crest of the discrete wave component and T_s is the time elapsed since the generation of the swell, henceforth denoted as the swell age. D_{xx}, D_{yy} and D_{xy} are the corresponding constituents of the diffusion tensor in Cartesian space, and c_x and c_y are the corresponding components of $\vec{c}_x - \vec{v}$. $\Delta\theta$ is the discrete directional increment in spectral space, and Δc_g is the increment in the group velocity corresponding to the discrete increment Δf in spectral space. Note that Booij and Holthuijsen (1987) derive their equations for a fixed grid with

$\vec{v} \equiv 0$. The modification for a grid moving with a given velocity $\vec{v}$ again is trivial, as in Eq. (2). Note also that the dependence of F on f and θ has been omitted here for brevity of notation.

Originally, Eqs. (4)–(9) have been implemented with the UQ scheme in WAVEWATCH III as a separate diffusion step in the fractional step method used to solve the model equations,

$$\frac{\partial F}{\partial t} = \frac{\partial}{\partial x}\left[D_{xx}\frac{\partial F}{\partial x}\right] + \frac{\partial}{\partial y}\left[D_{yy}\frac{\partial F}{\partial y}\right] + 2D_{xy}\frac{\partial^2 F}{\partial x \partial y}. \tag{10}$$

Furthermore, following the suggestion of Booij and Holthuijsen (1987), the diffusion is not increased with swell age T_s, but is kept constant to avoid numerical complications. Note that this implies that the diffusion is generally too strong near the generation area of the swell field (actual T_s smaller than average T_s), and too weak far away from the generation area (actual T_s larger than average T_s).

Although this GSE alleviation method has worked very well in the WAVEWATCH III model, it has been shown to have a practical disadvantage; Eq. (10) requires much smaller numerical time steps than Eq. (3) for high-resolution models, making the numerical solution much more expensive. To avoid this decrease in numerical time step, a spatial averaging techniques was introduced as a proxy for the diffusion equation (10) in version 2.22 of WAVEWATCH III (Tolman, 2002a,b). The area around each grid point over which the spatial averaging is performed extends in the propagation ($\vec{s}$) and normal ($\vec{n}$) directions as

$$\pm\gamma_s \Delta c_g \Delta t \vec{s}, \quad \pm\gamma_n c_g \Delta\theta \Delta t \vec{n}, \tag{11}$$

where γ_s and γ_n are tunable constants. Note that γ_s and γ_n, like T_s, are kept constant during the computation. Instinctively, one might expect that ideally $\gamma_s = \gamma_n = 1$. However, practical experience shows that the size of the averaging area should increase with T_s as in Eqs. (8) and (9). Hence, choosing constant factors γ will have a similar effect as choosing a constant T_s, that is, the near field solution will be smoothed too much, and the far field solution will be smoothed too little. This averaging technique now is the default approach in WAVEWATCH III, and has been used exclusively in the tests presented below.

The question to be answered is if the moving grid influences the GSE and its alleviation method(s). The straightforward incorporation of the grid advection in the Booij and Holthuijsen (1987) method Eqs. (4)–(9) suggests that no modifications are necessary. For the averaging technique, this is not instinctively clear, because the movement of the grid influences the characteristic velocities and directions of individual spectral components, and hence might influence the orientation and extend of the averaging areas. This is, however, not the case, as is illustrated in Fig. 1.

Fig. 1 shows a clear impact of the motion of the grid on the characteristic velocities of discrete spectral components relative to the moving grid. Without grid motion (panel a), the characteristics show the expected symmetric pattern. With substantial grid motion (panel b), the characteristics show a clear asymmetric pattern. Nevertheless, with grid motion, the end points of the characteristic vectors remain on concentric circles, in essence identical to the pattern for the case without grid motion. Hence, the ideal averaging areas also remain unchanged. Thus, the averaging technique can, in principle, also be applied to the moving grid case without modifications.

However, Fig. 1b also identifies a potential asymmetry in the GSE alleviation methods. Wave components moving to the right have a decreased advection velocity relative to the grid, whereas components moving to the left have an increased advection velocity. Hence, wave components

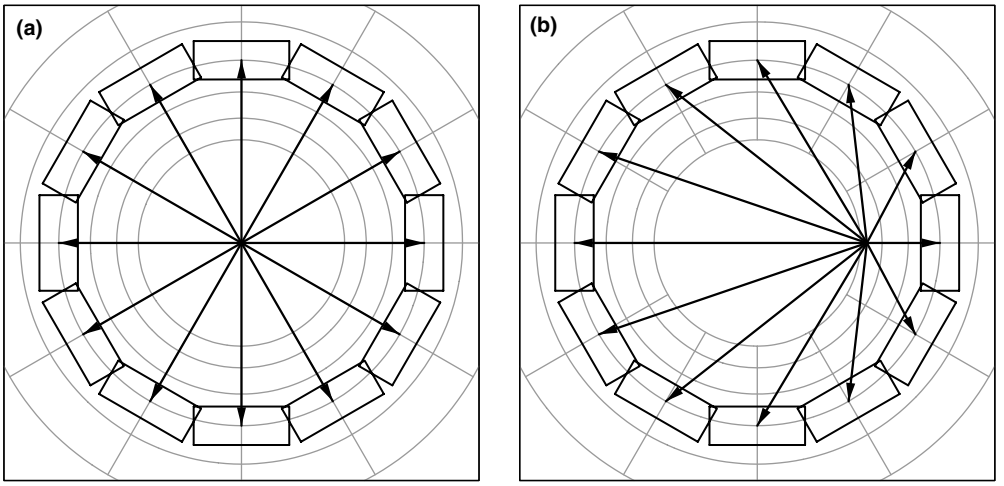

Fig. 1. Characteristic velocity vectors for 12 discrete directions and a single discrete frequency relative to the moving grid for (a) a stationary grid and (b) a grid moving with 60% of the corresponding group velocity to the right. All end points of the vector are located on a circle. Intersections of gray circles and lines correspond to solutions for other frequencies. Discrete frequencies representative for box areas as assumed in the GSE alleviation technique using spatial averaging (Eq. (11)) with $\gamma_s = \gamma_n = 1$.

moving to the right have an increased retention time in the grid, while components moving to the left have a reduced retention time. Because the GSE alleviation methods used here become less effective with the age of swell fields (or in this case, with retention time in the wave model), it may be expected that components moving to the right in Fig. 1b will show a more pronounced GSE than components moving to the left. Considering that the strengths of the diffusion and hence the factors γ ideally increase linearly with time, a more symmetric GSE alleviation for a moving grid can be obtained by replacing Eq. (11) with

$$\pm\gamma_a\gamma_s\Delta c_g\Delta t\vec{s}, \quad \pm\gamma_a\gamma_n c_g\Delta\theta\Delta t\vec{n}, \tag{12}$$

$$\gamma_a = \left(\frac{|\vec{c}_x|}{|\vec{c}_x - \vec{v}|}\right)^p, \tag{13}$$

where p is a tuning parameter. For $p = 0$ no correction is applied, whereas for $p = 1$ the averaging area is scaled linearly with the retention time of the spectral component in the moving grid. Note that Eq. (13) includes a singularity where $\gamma_a \to \infty$. In WAVE WATCH III this singularity is automatically dealt with because the averaging area is limited to the nine-point grid stencil surrounding the grid point in question.

5. Numerical testing

To illustrate the potential of the moving grid version of WAVEWATCH III, and particularly the impact of the GSE and its alleviation, a simple tropical cyclone test is considered. In this test, a model domain of 3000×3000 km is resolved with a spatial resolution of 25 km (123×123 grid

points). The spectrum is resolved with 25 frequencies (0.042–0.42 Hz, with 10% increments) and 24 directions ($\Delta\theta = 15°$), as in most common WAVEWATCH III applications. The wind field is described with a Rankine vortex

$$U_{10} = \begin{cases} rU_{\max}/R & \text{for } r < R, \\ U_{\max}/r & \text{for } \geqslant R, \end{cases} \tag{14}$$

where $U_{\max}$ is the maximum azimuthal wind speed, R is the radius of maximum wind and r is a radial coordinate relative to the center of the vortex, which is placed at the center of the grid, and moves with it. The wind directions are tangent to circles centered on the center of the vortex. The maximum wind speed and radius of maximum wind are set to $35\,\mathrm{ms}^{-1}$ and 100 km, respectively. To furthermore improve radial symmetry in the resulting wave field for stationary systems, the wind speed is set to 0 for radii $r > 1500$ km. This wind field is not corrected for the motion of the grid, and hence will remain symmetrical throughout the calculations.

The standard settings of the wave model WAVEWATCH III version 2.22 are used, with the exception of the use of $\gamma_s = \gamma_n = 2.0$ in Eq. (11) (unless specified differently). All time steps in the model are set to 900 s, with the exception of the minimum source term time step, which is set to 60 s (see Tolman, 2002b, Section 3.1 for details). The model is run for two days starting from initial conditions calculated from the wind fields (using default setting of WAVEWATCH III), and results at the end of the runs are presented.

Fig. 2a shows wave heights for a stationary cyclone. The results are nearly symmetric, with a clear GSE for the swell fields away from the center of the cyclone. Due to the GSE, wave height contours show wiggles instead of concentric circles. Note that this test is set up explicitly to display the GSE, and that the grid extends 500 km beyond the figure boundaries in each direction.

Fig. 2b shows resulting wave heights when the grid (and hence the wind field) are moved with a speed $\vec{v} = 5\ \mathrm{ms}^{-1}$ to the right, and with the original setup of the GSE alleviation technique ($p = 0$

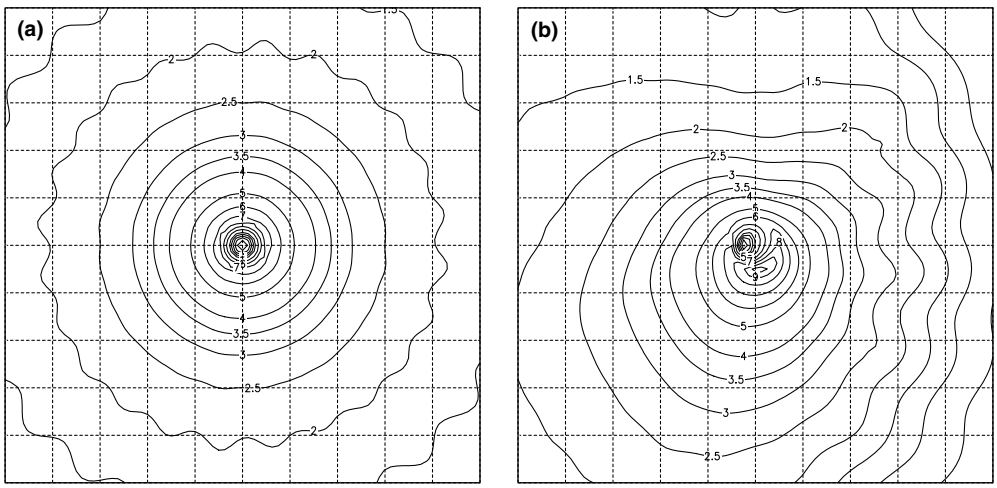

Fig. 2. Wave heights in (m) from idealized tropical cyclone test after two days of model integration. Grid lines at 200 km intervals with center of cyclone at center of grid. (a) Stationary cyclone, (b) cyclone and grid moving with $\vec{v} = 5\ \mathrm{ms}^{-1}$ to the right. No correction applied to GSE alleviation strength ($p = 0$).

in Eq. (13)). Compared to the stationary case, the GSE has increased in strength in the propagation direction of the cyclone (right side of Figure), and has virtually disappeared in the directions opposite to the propagation direction of the cyclone (left side of Figure). This was expected considering the longer retention time in the model of waves moving to the right, as discussed in the previous section. Note that the moving grid approach was independently validated using a stationary expanded grid with the corresponding moving wind fields defined at 15 min intervals. As expected, the results are virtually identical to Fig. 2b, including all details of the GSE (figure not presented here). This implies that previous validation results of WAVEWATCH III for hurricanes as presented in, for instance, Moon et al. (2003), are directly applicable to the moving grid version of the model, as long as the wave field is dominated by wind waves, and the wind field is properly contained within the moving grid.

The GSE can be made more symmetric than is the case in Fig. 2b by setting $p > 0$ in Eq. (13). Results obtained with $p = 1$ and $p = 0.5$ are presented in Fig. 3a and b, respectively. As discussed in the previous section, results of Booij and Holthuijsen (1987) indicate that ideally $p = 1$. The corresponding model results (Fig. 3a) indeed show a more or less symmetric display of the GSE relative to the center of the moving cyclone.

However, it is not necessarily desirable to balance the GSE for all propagation directions. In the moving cyclone case used here, the wave field generally extends over much larger areas behind the cyclone than in front of it. The correction with $p = 1$ then will leave the wave field behind the cyclone sensitive to the GSE. In such a case the correction can be reduced by choosing a smaller p. Fig. 3b shows the corresponding results for $p = 0.5$. The GSE now occurs somewhat asymmetrically, with a stronger GSE in front of the cyclone than behind it. The GSE is nevertheless more evenly distributed than in the case without the grid movement correction (Fig. 2b) as expected.

So far, the tests have used spatial averaging coefficients γ_s and γ_n chosen explicitly to display the GSE. Fig. 4 shows the results in which sufficient smoothing was introduced to eliminate the GSE for practical purposes. For the present case, this requires $\gamma_s = \gamma_n = 3.0$. Only marginal effects of the GSE can be observed, and for practical purposes the GSE has been eliminated.

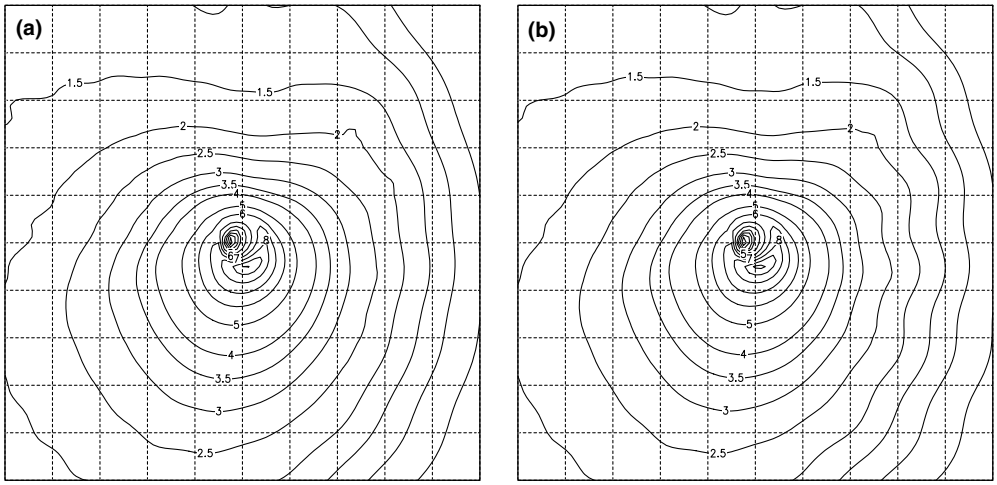

Fig. 3. Like Fig. 2b with GSE averaging correction of Eqs. (12) and (13). (a) $p = 1$. (b) $p = 0.5$.

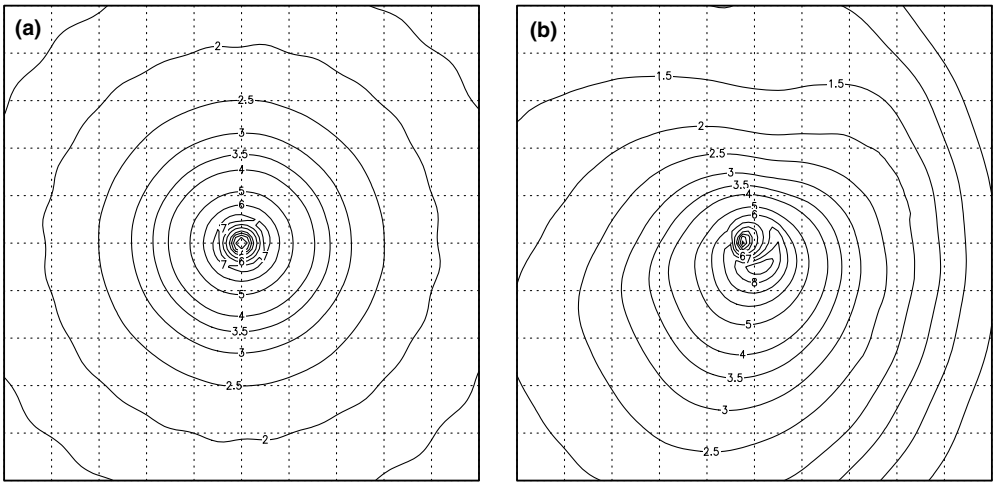

Fig. 4. Like Fig. 2 with $\gamma_s = \gamma_n = 3.0$ and $p = 0.5$ in Eqs. (12) and (13).

One note of caution needs to be made regarding the smoothing. Whereas the smoothing effectively removes the GSE and appears to have small impact on the solution away from the center of the cyclone, it is having a distinct impact on the wave height near the center of the cyclone. This is illustrated in Fig. 5, which shows model results without smoothing (panel a, $\gamma_s = \gamma_n = 0$) or with heavy smoothing (panel b, $\gamma_s = \gamma_n = 4.0$) near the center of the cyclone (note the different spatial scale compared to the previous figures). Both the maximum wave heights in the lower right quadrant of the cyclone, and the lowest wave height in the upper left quadrant are distinctly influenced by the smoothing. Away from the center, however, the differences between the resulting wave heights are moderate, and are dominated by the first signs of the GSE in the front of the cyclone.

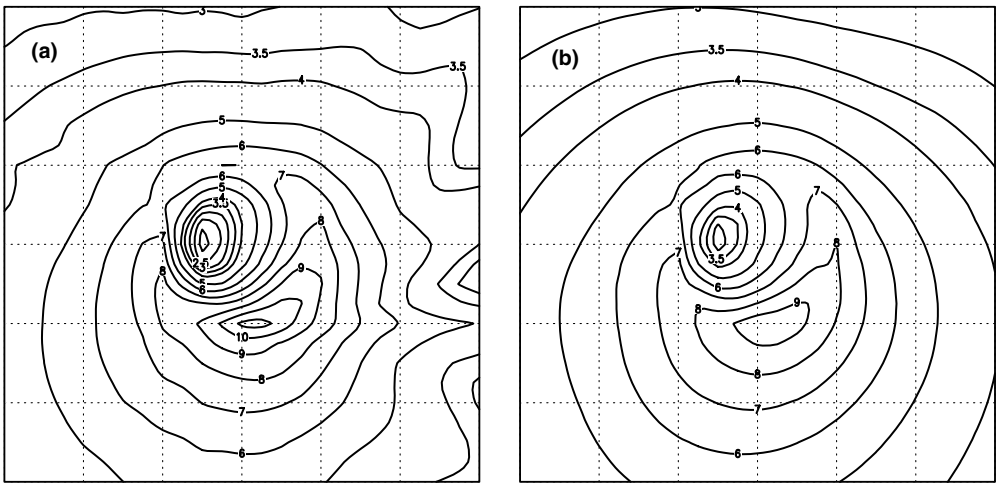

Fig. 5. Moving cyclone solution corresponding to Fig. 4b near the center of the cyclone without GSE mitigation (panel a, $\gamma_s = \gamma_n = 0$) or with strong mitigation (panel b, $\gamma_s = \gamma_n = 4.0$). Grid lines at 100 km intervals.

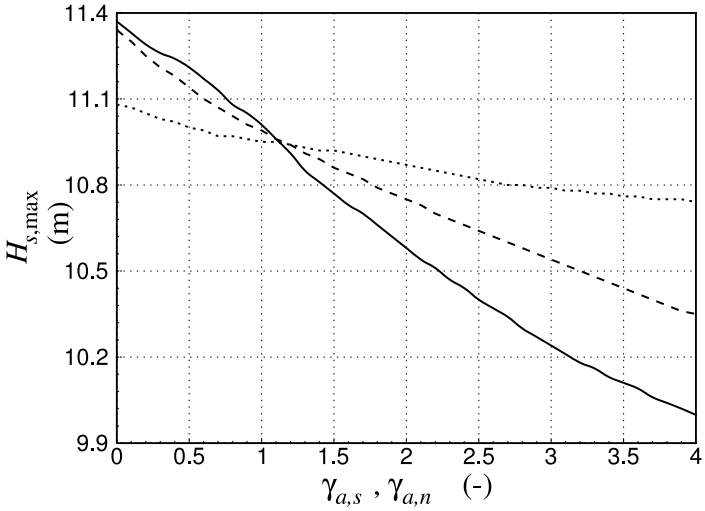

Fig. 6. Maximum wave height $H_{s,\max}$ (solid line) corresponding to the test case of Fig. 5 as a function of the smoothing parameters γ_s and γ_n in Eq. (12), $p = 0$. (Dashed and dotted lines) corresponding results for spatial grid resolution increased from 25 km to 12.5 and 6.25 km, respectively.

The impact of the smoothing is quantified in Fig. 6, which shows the maximum wave height as a function of the smoothing parameters γ_s, and γ_n. By increasing the smoothing factors from 0 to 4, the maximum wave height reduces systematically by up to 15% (solid line). However, this sensitivity is for a significant part due to the relatively poor spatial resolution of the test case used here. This is illustrated in Fig. 6 with the corresponding results obtained with models with a spatial resolution of 12.5 and 6.25 km (dashed and dotted lines, respectively). In the latter case, the maximum wave height varies by only 3% over the range of smoothing parameters considered.

6. Hurricane Lili

So far, the moving grid model has only been applied to idealized wind fields. The model is also easily applied to more realistic (hurricane) wind fields from models or analyses, as long as the storm is sufficiently far from land, and in sufficiently deep water. This will be illustrated here with simulations of the wave field generated by hurricane Lili in the Gulf of Mexico in early October 2002. Considered is the period from 1800 UTC on October 1 through 0000 UTC October 4, when Lili was effectively in the Gulf of Mexico and mostly in deep water. Wind field analyses produced with the H*Wind package (Powell et al., 1996, 1998) by the Hurricane Research Division (HRD) of the Atlantic Oceanographic and Meteorological Laboratory (AOML) of NOAA are used to perform the wave model simulations. All data used here have been obtained from the HRD web site. [1] The H*Wind analyses are produced interactively, requiring human intervention. Generally, they are available for hurricanes at six hour intervals. For Lili, and for the period

[1]

considered here, however, they are available at regular three hour intervals, from 1200 UTC on September 27 through 1200 UTC on October 4. The H*Wind wind fields are used in combination with the three hourly track data from the Tropical Prediction Center (TPC) of NOAA. [2] Note that these two data sources are mutually consistent with respect to the position of Lili.

Two wave models have been set up to be used with these wind fields. The first is a conventional (fixed grid) model, covering the entire Gulf of Mexico with a Cartesian deep water grid and a spatial resolution of approximately 10 km. The second is a moving grid model with an identical spatial resolution, centered on the eye of the hurricane, and with a nearly circular domain with a radius of approximately 300 km. Both models use the spectral resolution as in the previous tests. The four model time steps are set to 300, 100, 300 and 30 s, respectively (see Tolman, 2002b, Section 3.1 for details), and the smoothing factors in the GSE alleviation, are set to $\gamma_s = \gamma_n = 2.0$, and $p = 0.5$ in the moving grid model.

Both models use wind fields from H*Wind only. First, these winds are interpolated onto a storm-centered moving circular grid. Such winds are used directly in the moving grid model. The corresponding grid advection velocity $\vec{v}(t)$ is calculated from consecutive track points, and is kept constant between consecutive track points (and times). Second, the fixed model wind fields are obtained by interpolating the moving grid winds to the larger fixed grid domain, using the appropriate track location. Wind speeds in the fixed grid outside the moving circular domain are assumed to be zero. Thus, both models use wind fields that in principle are identical, with the exception of some loss of information (extreme values) when the moving grid winds are interpolated once more onto the fixed grid. Both wind fields have a time resolution of three hours. Because such analyses in many cases are available only at six hour intervals, six hourly wind fields were obtained by skipping every other H*Wind analysis, starting at 0300 UTC.

Apart from the grid size and motion, the main difference between the models is the way in which the wind fields are interpolated in time inside the wave model. In the moving grid model, the wind field is always centered on the eye of Lili, resulting in hurricane wind fields that remain unaffected by spatial aliasing at any time step of the wave model. For the conventional fixed grid model, Lili shows a significant spatial displacement between consecutive wind field analyses, particularly when they are available only with a six hour time resolution. The corresponding interpolated wind fields at model time steps in between the times at which the analyses are available then suffer from the effects of spatial aliasing. This is illustrated in Fig. 7 with wind fields for both models valid at 2100 UTC on October 2 as obtained from six hourly H*Wind wind fields. This valid time is halfway between two consecutive H*Wind wind fields. In the moving grid model (Fig. 7a), the time interpolation of the winds results in a consistent and realistic hurricane wind field, with a well defined circulation, and a distinct eye at the center of the grid. For the fixed grid model (Fig. 7b), wind fields are clearly unrealistic, displaying two wind speed maxima (corresponding to the locations of the hurricane in the two analyses used), and no realistic circulation. Furthermore, maximum wind speeds are severely underestimated.

Unrealistic wind speeds lead to unrealistic wave fields. This is illustrated in Fig. 8 with wave height fields corresponding to the wind fields presented in Fig. 7. Wave heights in the moving grid model (Fig. 8a) are higher, and display the expected distribution with maximum wave

[2] http://www.nhc.noaa.gov/.

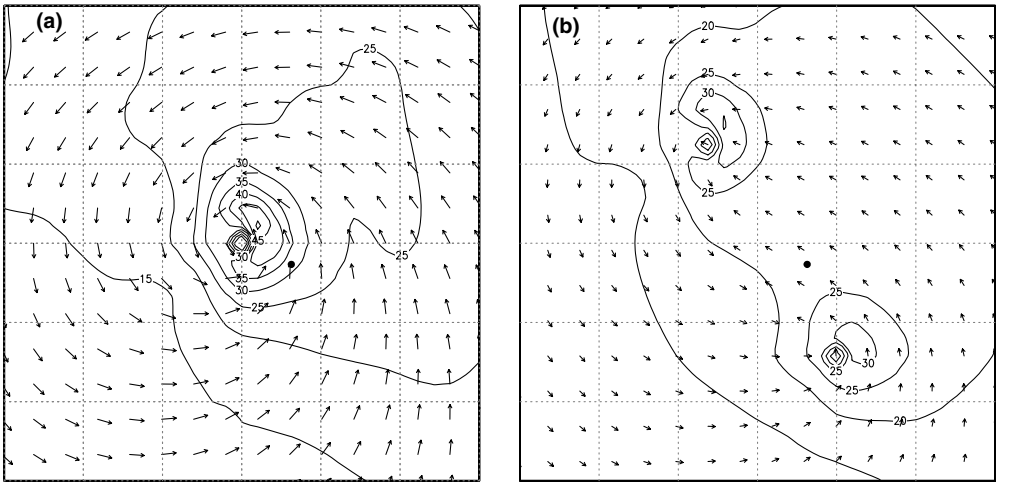

Fig. 7. Wind speeds U_{10} in ms^{-1} for Lili at October 2, 2100 UTC for the moving grid model (panel a) and the fixed grid model using six hourly H*Wind wind fields three hours before and after valid time. Grid lines at 50 km intervals, contour lines at $5\,ms^{-1}$ intervals. (●) Location of buoy 42001.

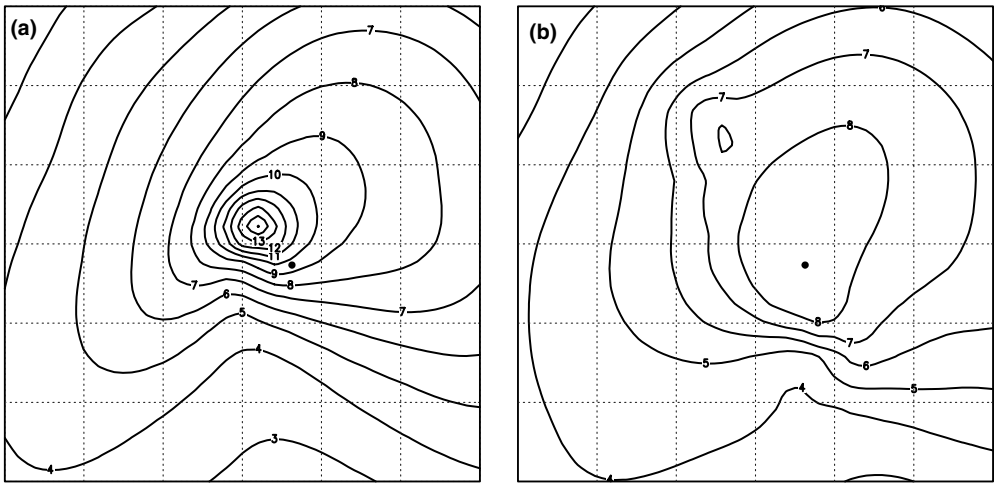

Fig. 8. Wave heights H_s in m corresponding to wind speeds and models of Fig. 7. Contours at 1 m intervals.

heights in the front right quadrant, whereas wave heights in the fixed grid model (Fig. 8b) are lower, and display a less consistent spatial distribution. Rather than propagating the maximum wave heights continuously near the track, the fixed grid model develops a set of consecutive discrete locations with maximum wave heights, corresponding to the discrete locations of Lili in the analyzed wind fields. In Fig. 8b, the development of a new local wave maximum is evident in the northwest quadrant of the $H_s = 7$ m contour, and the corresponding closed $H_s = 8$ m contour (not labeled).

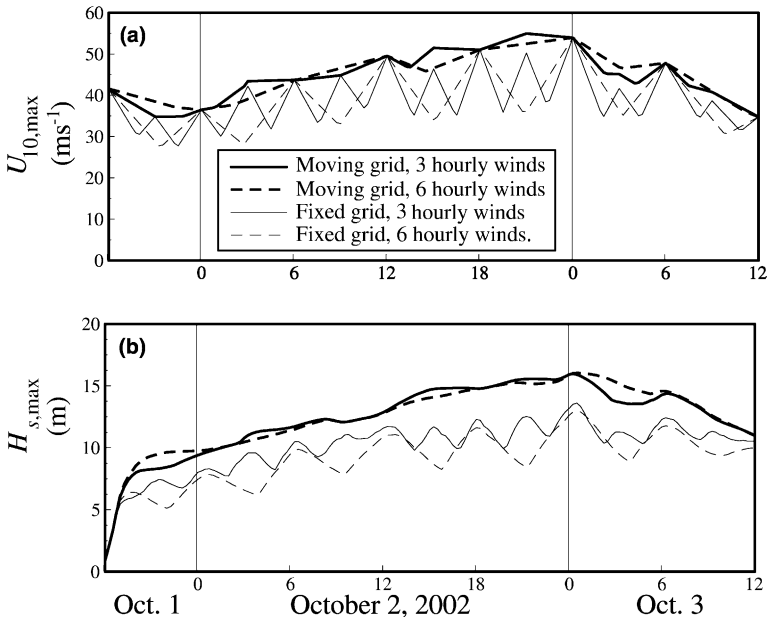

Fig. 9. Maximum wind speeds U_{10} (panel a) and wave heights H_s (panel b) for the simulation period from the moving and fix grid models for three and six hourly wind fields, respectively.

The large impact of the modeling approach on the quality of the wind fields, and hence on the quality of the wave fields is furthermore illustrated in Fig. 9, which presents the maximum wind speeds and wave heights throughout the model domains for the entire simulation period. For the moving grid model (thick lines), the three or six hourly availability of H*Wind data has only a minor impact on the wind speed and wave height maxima, and is related to the gain (loss) of wind speed information through the added (removed) analyses. For the fixed grid model, maximum wind speeds at the valid times of the available H*Wind data are generally close to those of the moving grid model (compare solid lines or dashed lines). However, in particular at 1500 UTC and 2100 UTC on October 2, the maximum winds for the fixed grid model (thin solid line) are significantly lower than those of the moving grid model (thick solid line). This is due to the additional interpolation step from the moving to the fixed grid as described above, and implies that the 10 km grid resolution used here is not always adequate to properly describe the wind field in Lili. At interpolation times in between these valid times the fixed grid wind speed maxima are always significantly lower than for the moving grid, due to the aliasing problem illustrated in Fig. 7. The aliasing problem obviously is larger for the six hourly wind fields (dashed thin line in Fig. 9a) than for the three hourly wind fields (solid thin line). The lower maximum wind speeds in the fixed grid model result in significantly lower maximum wave heights as would be expected (Fig. 9b), even at the valid times of the wind fields, when the wind fields are properly represented.

The lower wind speeds and wave heights in the fixed grid model are mostly an artifact of the aliasing in the wind field interpolation in time. This problem can be alleviated by providing the fixed grid model with realistic wind fields with a better resolution in time. For hurricanes like Lili, such wind fields can be generated by interpolating wind fields in time relative to the storm center,

and displacing them in space along the storm track, as is naturally done in the moving grid models. Fixed grid model results with such wind fields with increasing time resolution are much closer to the results of the moving grid model, but remain somewhat lower due to the additional interpolation onto the fixed grid (figures not presented here).

Fig. 10 presents wave height and wind speed data observed at buoy 42001 in the center of the Gulf of Mexico. Lili moved directly over this buoy, with maximum wind speeds and wave heights observed on October 2 at 2100 UTC and 2200 UTC, respectively. The moving grid model provides data only when buoy 42001 is located inside the grid. The fixed grid would normally provide non-zero wind and wave data for the entire period. However, because winds outside the hurricane analyses used in the moving grid are ignored, fixed grid winds and waves are not produced until the hurricane winds reach the buoy location. Due to the lack of background wave conditions, both models need to "catch up" to the wave conditions initially, and appear to have done so when hurricane winds start to increase after 1600 UTC on Oct. 2. The major difference between the models occurs in extreme conditions when Lili's maximum winds are over buoy 42001. The moving grid model shows a clear overestimation of the maximum wave heights observed at buoy 42001 (compare solid lines and symbols in Fig. 10b), whereas the wind field appears to be well represented. This overestimation is consistent with apparent overestimations of wind stresses (and hence wave growth) in the wave model for wind speeds above $15\,\mathrm{ms}^{-1}$ (e.g., Powell et al., 2003; Tolman et al., 2004; Moon et al., 2005). The fixed grid model shows an underestimation of maximum wave conditions, as the above deficiencies in the wave model physics are over compensated by the aliasing deficiencies of the wind field.

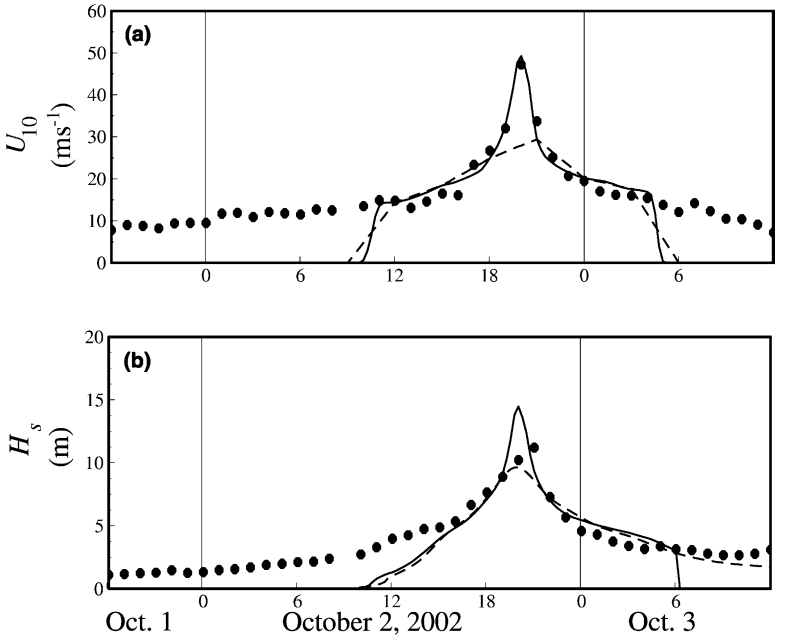

Fig. 10. Wind speed U_{10} (panel a) and wave height H_s (panel b) at buoy 42001 in the center of the Gulf of Mexico. (●) Observations, (solid lines) moving grid model with three hourly wind data, (dashed lines) fixed grid model with three hourly wind data.

Finally, it should be noted that the main reason of developing the moving grid model is to increase the economy of modeling waves near hurricanes. In the tests for Lili, the moving grid model incorporates a factor of 6.8 less grid points, and requires on average a factor of 4 less run time. The speed up in run time for the moving grid model would have been even more favorable if realistic winds would have been used through the fixed model grid. In the latter case, wave growth throughout the fixed grid model would require addition computing time. Note furthermore that both the grid point and run time ratios will favor a moving grid model even more if hurricanes move through larger basin like the North Atlantic Ocean.

7. Discussion and conclusions

The present study presents a version of the WAVEWATCH III wave model featuring a moving grid option. This model version is intended for research into waves generated by tropical systems in deep water conditions away from the coast. This model could also be used to assess waves generated by extra-tropical systems and fronts, because it allows for much higher spatial resolutions than is attainable with conventional models. For hurricane Lili in the Gulf of Mexico, the moving grid approach reduced the number of model grid points by a factor of 6.8, and the model run time by a factor of 4, compared to a conventional fixed grid model. For applications in larger basins, these ratios are expected to favor the moving grid model even more.

With the simplifications of deep water and no coastlines, the required modifications to the wave model code are fairly trivial. Most complications occur in the alleviation of the Garden Sprinkler effect (GSE). It is shown that, in principle, the GSE alleviation techniques do not need to be modified in the moving grid approach. However, deficiencies in GSE alleviation methods, where the alleviation is more efficient for younger swells than older swells, lead to an apparent reintroduction of the GSE for waves traveling ahead of the tropical system. This can be remedied by modifying the strength of the GSE alleviation as a function of the wave propagation direction and speed relative to the motion of the grid, as in Eqs. (12) and (13).

It should be noted that the apparent asymmetry of the GSE is due to the general characteristics of a moving hurricane, and that this behavior occurs independent of the movement of the grid (see discussion of Fig. 2). The GSE alleviation correction as introduced in Eqs. (12) and (13) presents an elegant way to remove this asymmetry. Such an approach can only be used relatively close to a dominant storm system, and is therefore not generally applicable to conventional large scale models. This approach can tentatively be applied in other localized grids such as the relocatable grid approach as discussed in Section 1. The applicability of asymmetric GSE alleviation in local grids should be considered as a significant advantage, and as an additional benefit for modeling hurricanes with local grid systems.

Test results clearly indicate that the amount of smoothing used to alleviate the GSE has a distinct impact on the model results, with different impacts near the center of the cyclone or away from it. This suggests that the selection of the smoothing parameters γ_s and γ_n should depend on the focus of the study performed.

If the study concentrates on the 'near field' wave heights generated by the cyclone, either sufficient spatial resolution or small smoothing factors are required to obtain realistic results. If the spatial resolution is limited, excessive smoothing will influence the maximum and minimum

wave heights near the center of the cyclone notably (and spuriously). This is illustrated here with results presented in Figs. 5 and 6. Note that in this test, the radius of maximum winds (100 km) is not well resolved by the spatial grid increment (25 km).

If the 'far field' solution is sought after, that is, wind seas in regions with weaker winds and the swell field away from the cyclone, the amount of smoothing applied needs to be sufficient to remove the GSE. The present results suggest that the impact on the corresponding wave heights would be much less than for the maximum (near field) wave height.

For general idealized studies, this suggests that it might be necessary to run several models with different numerical setting to obtain a complete and reliable picture of the wave fields associated with a cyclone. It should also be noted that the development of a multiple nested wave model, as presently used in atmospheric modeling of hurricanes (see Section 1), provides a natural way to increase the amount of smoothing the innermost grid to the outer grid(s). The most elegant solution, however, would be to either implement the Booij and Holthuijsen (1987) diffusion, or Tolman (2002a) averaging approach with a dynamically adjusted swell age T_s, as originally envisioned by Booij and Holthuijsen (1987). Alternatively, the divergent flux approach suggested by Tolman (2002a) could be developed to maturity. Both alternatives, however, are expected to be more computationally expensive than the present GSE alleviation methods.

It should also be noted that in Fig. 5a, that is, the model run without GSE alleviation, the most pronounced effects of the GSE occur for waves traveling to the right along a spatial grid line originating at the radius of maximum wind (100 km below the eye of the cyclone, which is at the center of the grid). The occurrence of preferred propagation directions has been observed before for models using first order propagation schemes without additional GSE alleviation (Bidlot et al., 1997; Phadke et al., 2003). For the third order scheme with GSE alleviation, directional preferences along the spatial grid axes are virtually non-existent, as is obvious from Figs. 2 and 4a, particularly when these results are compared with a similar test with a first order scheme in Phadke et al. (2003), their Fig. 7a. Such a directional preference can be mitigated by rotating the discrete spectral direction away from the spatial grid axes as demonstrated by Bidlot et al. (1997). Although apparently not necessary for the third order scheme used in WAVEWATCH III, the shifting of the direction over the range $\pm\frac{1}{2}\Delta\theta$ has been added to the present test version of the model as an option for the user.

Fixed and moving grid models in Section 5 showed identical results (with fixed grid wind fields provided for each time step of the model). Hence, previous validation data for WAVEWATCH III in hurricane conditions (see Section 1) are in principle applicable to the moving grid version, as long as the fixed grid validations did not suffer from wind interpolation problems as discussed in Section 6 and below.

The present study provides additional validation data for hurricane Lili in the Gulf of Mexico in 2002, using analyzed H*Wind wind fields from AOML/HRD. Such analyzed wind fields are typically available at high spatial resolution, but at poor temporal resolution (three or six hour intervals). By keeping the eye of Lili centered on the grid, the moving grid version of the wave model provides a natural way to interpolate hurricane wind fields in time. Conversely, a conventional time interpolation in fixed grids leads to unrealistic wind and wave fields due to spatial aliasing, as is illustrated in Figs. 7–9. Because interpolation errors can only reduce wind speeds, such errors systematically and spuriously reduce maximum modeled wind speeds and wave heights.

The moving grid model overestimates the maximum wave height observed at buoy 42001, although wind speeds do not appear to be overestimated. Recent observations and model validation suggest that this represents a systematic model error in WAVEWATCH III (and other third generation wave models), that is related to the overestimation of wind stresses for hurricane wind speeds (see discussion in Section 6).

Conversely, the fixed grid model underestimates the maximum wind speed and wave height, due to the above mentioned wind interpolation errors. Consequently fixed grid hurricane wave models appear to suffer from two main errors. The first is the overestimation of wave growth due to the overestimation of wind stresses in the wave growth parameterization for extreme wind speeds. The second is the underestimation of wind speeds due to interpolation in time of wind fields. These errors will partially cancel. In an operational wave model such a cancellation of errors is beneficial for the quality of the present forecast product. From a scientific perspective, this is detrimental, as the wind speed interpolation error tends to mask the shortcomings of the parameterization of wave growth physics. Because the wind interpolation error is naturally minimized in the moving grid model, such a model appears much more naturally suitable for investigation into the wave model physics.

Acknowledgment

The author would like to thank D.B. Rao, H.S. Chen, Naomi Surgi and the anonymous reviewers for their constructive comments on early drafts of this manuscript.

References

Bao, J., Wilczak, J.M., Choi, J., Kantha, L.H., 2000. Numerical simulations of air–sea interaction under height wind conditions using a coupled model: a study of hurricane development. Monthly Weather Review 128, 2190–2210.

Bender, M.A., Ginis, I., 2000. Real-case simulations of hurricane-ocean interaction using a high-resolution coupled model: effects on hurricane intensity. Monthly Weather Review 128, 917–946.

Bender, M.A., Ross, R.J., Tuleya, R.E., Kurihara, Y., 1993. Improvements in tropical cyclone track and intensity forecasts using the GFDL initialization system. Monthly Weather Review 121, 2046–2061.

Bidlot, J.R., Janssen, P., Hansen, B., Guenther, H., 1997. A modified set up of the advection scheme in the ECMWF wave model. Technical memorandum 237, ECMWF, 31 pp.

Booij, N., Holthuijsen, L.H., 1987. Propagation of ocean waves in discrete spectral wave models. Journal of Computational Physics 68, 307–326.

Chalikov, D.V., Belevich, M.Y., 1993. One-dimensional theory of the wave boundary layer. Boundary Layer Meteorology 63, 65–96.

Chao, Y.Y., Tolman, H.L., 2000. Numerical experiments on predicting hurricane generated wind waves. In: Preprints 6th International Workshop on Wave Hindcasting and Forecasting, pp. 167–179. Environment Canada.

Chao, Y.Y., Tolman, H.L., 2001. Specification of hurricane wind fields for ocean wave prediction. In: Edge, B.L., Hemsley, J.M. (Eds.), Ocean Wave Measurement and Analysis. ASCE, pp. 671–679.

Chao, Y.Y., Burroughs, L.D., Tolman, H.L., 2003. The North Atlantic Hurricane wind wave forecasting system (NAH). Technical Procedures Bulletin 478, NOAA/NWS. Available from: <http://polar.ncep.noaa.gov/mmab/tpbs/tpb478/tpb478.htm>.

Gopalakrishnan, S.G., Bacon, D.P., Ahmad, N.N., Boybeyi, Z., Dunn, T.J., Mali, M.S., Jin, Y., Lee, P.C.S., Mays, D.E., Madala, R.V., Sarma, A., Turner, M.D., Wait, T.R., 2002. An operational multiscale hurricane forecasting system. Monthly Weather Review 130, 1830–1842.

Komen, G.J., Cavaleri, L., Donelan, M., Hasselmann, K., Hasselmann, S., Janssen, P.E.A.M., 1994. Dynamics and Modelling of Ocean Waves. Cambridge University Press, 532 pp.

Kurihara, Y., Bender, M.A., 1980. Use of a movable nested-mesh model for tracking a small vortex. Monthly Weather Review 108, 1792–1809.

Kurihara, Y., Tripoli, G.J., Bender, M.A., 1979. Design of a moveable nested-mesh primitive equation model. Monthly Weather Review 107, 239–249.

Kurihara, Y., Bender, M.A., Tuleya, R.E., Ross, R.J., 1995. Improvements in the GFDL hurricane prediction system. Monthly Weather Review 123, 2791–2801.

Leonard, B.P., 1979. A stable and accurate convective modelling procedure based on quadratic upstream interpolation. Computational Methods in Applied Mechenical Engineering 18, 59–98.

Leonard, B.P., 1991. The ULTIMATE conservative difference scheme applied to unsteady one-dimensional advection. Computational Methods in Applied Mechenical Engineering 88, 17–74.

Moon, I.J., Ginnis, I., Hara, T., Tolman, H.L., Wright, C.W., Walsh, E.J., 2003. Numerical modeling of sea surface directional wave spectra under hurricane wind forcing. Journal of Physical Oceanography, 33, 1680–1706.

Moon, I.J., Hara, T., Belcher, I.G.S.E., Tolman, H.L., 2005. Effect of surface waves on air–sea momentum exchange. I. Effect of mature and growing seas. Journal of Atmospheric Sciences 61, 2321–2333.

Phadke, A.C., Martino, C.D., Cheung, K.F., Houston, S.H., 2003. Modeling of tropical cyclone winds and waves for emergency management. Ocean Engineering 30, 553–578.

Powell, M.D., Houston, S.H., Reinhold, T.A., 1996. Hurricane Andrew's landfall in south Florida. Part I: standardizing measurements for documentation of surface wind fields. Weather and Forecasting 11, 304–328.

Powell, M.D., Houston, S.H., Amat, L.R., Morisseau-Leroy, N., 1998. The HRD real-time hurricane wind analysis system. Journal of Wind Engineering and Industrial Aerodynamics 77–78, 53–64.

Powell, M.D., Vickery, P.J., Reinhold, T.A., 2003. Reduced drag coefficient for high wind speeds in tropical cyclones. Nature 442, 279–283.

Tolman, H.L., 1991. Effects of tides and storm surges on north sea wind waves. Journal of Physical Oceanography 21, 766–781.

Tolman, H.L., 2002a. Alleviating the Garden Sprinkler effect in wind wave models. Ocean Modelling 4, 269–289.

Tolman, H.L., 2002b. User manual and system documentation of WAVEWATCH III version 2.22. Tech. Note 222, NOAA/NWS/NCEP/MMAB, 133 pp.

Tolman, H.L., Balasubramaniyan, B., Burroughs, L.D., Chalikov, D.V., Chao, Y.Y., Chen, H.S., Gerald, V.M., 2002. Development and implementation of wind generated ocean surface wave models at NCEP. Weather and Forecasting 17, 311–333.

Tolman, H.L., Alves, J.H.G.M., Chao, Y.Y., 2004. A review of operational forecasting of wind generated waves by hurricane Isabel at NCEP. Tech. Note 235, NOAA/NWS/NCEP/MMAB, 45 pp.

Young, I.R., 1988. Parametric hurricane wave prediction model. Journal of Waterway, Port, Coastal and Ocean Engineering 114, 637–652.

Young, I.R., 1999. Wind Generated Ocean Waves. Elsevier, 288 pp.

Young, I.R., 2003. A review of the sea state generated by hurricanes. Marine Structures 16, 210–218.